

Fast spectrometer near the Heisenberg limit with direct measurement of time and frequency for multiple single photons

Jakub Jirsa,^{1,2} Sergei Kulkov,¹ Raphael A. Abrahao,³ Jesse Crawford,³ Aaron Mueninghoff,⁴ Ermanno Bernasconi,⁵ Claudio Bruschini,⁵ Samuel Burri,⁵ Stephen Vintskevich,⁶ Michal Marcisovsky,¹ Edoardo Charbon,⁵ and Andrei Nomerotski³

¹*Faculty of Nuclear Sciences and Physical Engineering,
Czech Technical University, 115 19 Prague, Czech Republic*

²*Faculty of Electrical Engineering, Czech Technical University, 166 27 Prague, Czech Republic*

³*Brookhaven National Laboratory, Upton NY 11973, USA*

⁴*Stony Brook University, Stony Brook NY 11794, USA*

⁵*École polytechnique fédérale de Lausanne (EPFL), CH-2002 Neuchâtel, Switzerland*

⁶*Technology Innovation Institute, Abu Dhabi, United Arab Emirates*

(Dated: April 25, 2023)

We present a single-photon-sensitive spectrometer, based on a linear array of 512 single-photon avalanche diodes, with 0.04 nm spectral and 40 ps temporal resolutions. We employ a fast data-driven operation that allows direct measurement of time and frequency for simultaneous single photons. Combining excellent temporal and spectral resolution, our result is only a factor of ten above the Heisenberg Uncertainty Principle limit of $\hbar/2$ for energy and time, despite the simplicity of our experimental setup. This work opens numerous applications in quantum photonics, especially when both spectral and temporal properties of single photons are exploited.

Despite remarkable advances in single-photon detection, modern optical technologies are reaching their limits when both the spectral and temporal resolutions are combined. This is especially true for applications desiring to approach the limits governed by the wave-particle duality in quantum mechanics, which can also be formulated as the Heisenberg Uncertainty Principle (HUP). We address some of these critical challenges in achieving single-photon detection sensitivity together with excellent spectral (sub-nanometer in wavelength) and temporal (picosecond scale) resolutions.

Different kinds of single-photon detectors have different technical performances and focus on different tasks. Common types of detectors are single-photon avalanche detectors (SPAD) [1–4], superconducting nanowire single-photon detectors (SNSPD) [5–10], and transition edge sensors (TES) [11–15]. SPAD detectors are widely used in quantum photonics due to their user-friendly operation and reasonable photon detection efficiency compared to their cost. Production of SPADs in a monolithic complementary metal-oxide-semiconductor (CMOS) process enables better electronics integration and fast digital control interface, also supporting outstanding temporal resolution and scalability [16]. Arranging the SPAD detectors in a linear array with easy access to individual pixels allows one to employ the external resources of field programmable gate arrays (FPGA) to perform the time stamping and other digital operations. Additionally, SPAD sensors work at room temperature, an important aspect of their ease of use. Combining these advances with excellent spectral resolution makes this quantum photonics tool highly compelling.

Such a detector can unlock new uses and applications in both classical and quantum optics, especially when

considering spectral binning and wide bandwidth applications. Here we present a spectrometer based on the LinoSPAD2 sensor [17] and test its features, hence confirming its qualities and delivering a nearly Heisenberg-limited performance. As an example, we aim to use the LinoSPAD2 spectrometer for quantum-assisted astronomy [18–20]. Other potential applications are in spectroscopy, atomic physics, and quantum photonics.

I. RESULTS

A. Fast single-photon spectrometer

A line of single-photon sensitive pixels with flexible, data-driven readout and excellent timing resolution is ideal for implementing a fast spectrometer for quantum applications. We start by sending a beam of collimated photons to a diffraction grating, then focusing the linear image of the spectrum onto the LinoSPAD2 sensor. Fig. 1 depicts a schematic of our experimental setup. We employed two light sources for the characterization of the spectrometer, a thermal light source and a spontaneous parametric down-conversion (SPDC) single-photon source, as explained in more detail in the next section.

In the LinoSPAD2 sensor, each pixel is a single-photon sensitive photodiode with a $26.2 \times 26.2 \mu\text{m}$ size and 25% fill factor. The sensor consists of a linear 512x1 pixel array with a median dark count rate (DCR) below 100 counts per pixel per second and a peak photon detection probability of approximately 50%. A second-generation device with microlenses achieves an additional improvement in sensitivity by a factor of 2.3 with final photon detection efficiency (PDE) of about 30% at 520 nm [17]. Each pixel in the array allows for single-photon detec-

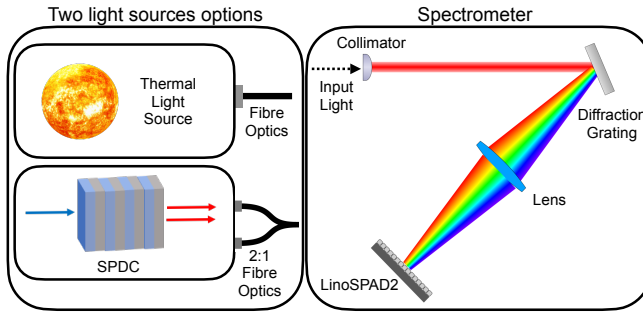


FIG. 1. Schematic layout of the spectrometer with two possible light sources used for evaluation of the spectral and temporal resolutions.

tion with time-stamping by employing FPGA processing. This ensures the reconfigurability of the LinoSPAD2 and permits adjustments in both the readout and processing chains, and in the spatial and temporal granularity, thus allowing one to match specific application requirements. Fig. 2 presents a photograph of the LinoSPAD2 sensor edge with about 20% of pixels shown.

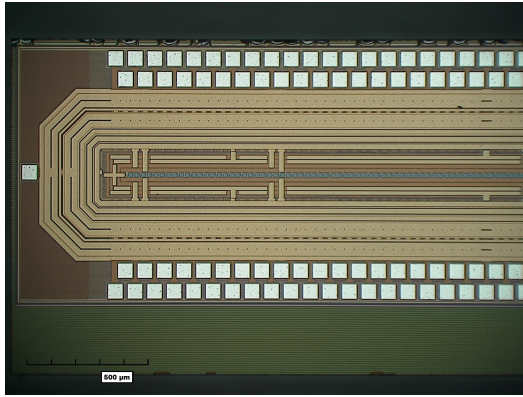


FIG. 2. Photograph of the LinoSPAD2 sensor edge with about 20% of pixels shown. The line of pixels is in the centre, oriented horizontally. The bonding pads on the top and bottom are used for connecting individual pixels to the FPGA on the motherboard. Reproduced from [17].

B. Spectrometer spectral and temporal resolutions

The spectrometer was characterized using the argon emission spectrum [21], corrected for transmission through air, which has a large number of narrow lines. A section of the resulting pattern after the diffraction grating with 1200 lines/mm is shown in Fig. 3. The peaks correspond to spectral lines of argon, which have well-known wavelengths and, therefore, provide excellent calibration for the spectrometer. The peaks are fitted with a Gaussian function to determine the spectral resolution (rms). Using a lens with $f = 200$ mm, we selected a

spectral range of 30 nm centered at 805 nm. Our best result was a spectral resolution of $\sigma = 0.04$ nm for the 800.61 nm line, while the spectral resolution varied between 0.04 and 0.05 nm. The total time to acquire the dataset was 400 s.

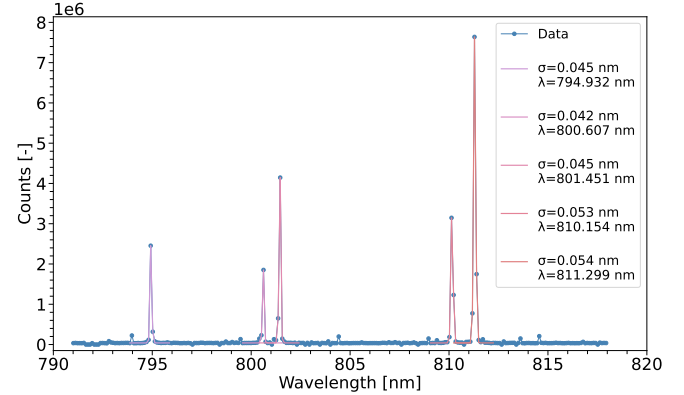


FIG. 3. Argon spectrum measured with LinoSPAD2.

We used a commercial spontaneous parametric down-conversion (SPDC) source of simultaneous photon pairs to characterize the timing resolution of the spectrometer [22, 23]. The idler and signal photons from the source were fiber-coupled and focused onto two separate locations on the sensor. Since the SPDC photons are generated simultaneously, they are ideal for timing calibration. Figure 4 shows the distribution of time differences for two-photon coincidence detection. Using a Gaussian fit, we obtain a temporal resolution (rms) of 57 ps for coincident counts. Assuming equal contributions to uncertainty for each of the two photons in the pair, we determine a temporal resolution of $57/\sqrt{2} = 40$ ps for a single photon, which is one of the best results ever reported for a single photon-sensitive spectrometer. The peak is centered at 18.3 ns due to different delays in the two arms of the SPDC source.

We note that for the purposes of resolution evaluation for both spectral and temporal measurements, we are far away from any quantum limitations. The natural temporal coherence of the argon lines is 150 ps [20] corresponding to the spectral width of picometers, which is much smaller than the measured spectral resolution. At the same time the simultaneity of SPDC photons is in 10's of femtoseconds given the 10 nm bandwidth of the source [23], which is much smaller than the current time resolution.

C. Characterization of simultaneous SPDC photon pairs

Since the sensor readout is data-driven and as such is completely independent for all pixels, it can register multiple photons simultaneously as long as they hit different pixels. To demonstrate this in the spectrometer setting,

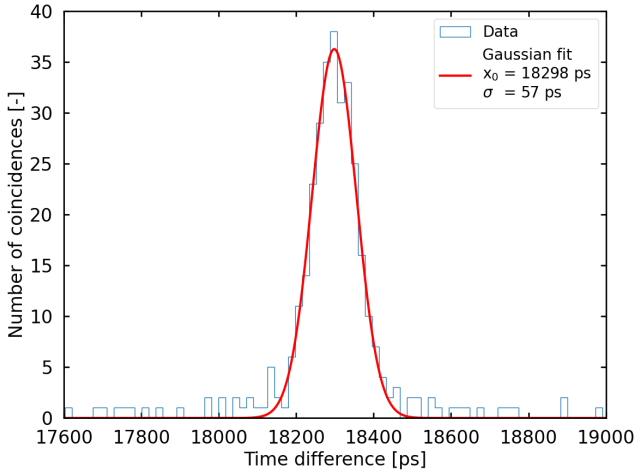


FIG. 4. Distribution of time differences for two-photon coincidence detection from a SPDC source.

the idler and the signal photons were combined using a 2:1 fiber splitter and then directed through the spectrometer in the same optical path as the argon thermal light. The SPDC signal and idler have different non-degenerate spectra [23], therefore, the diffracting grating will cause them to reach different pixels in the LinoSPAD2.

To prove that the spectrometer is sensitive to simultaneous pairs of photons, we analyzed their spectrum in our spectrometer, and the result is shown in Fig. 5 for the case of SPDC pump power of 50 mW. There are two wide peaks in the distribution corresponding to the spectra of signal and idler photons. The left and right peaks are the signal and idler photons, respectively, which were determined from previous measurements [23, 24].

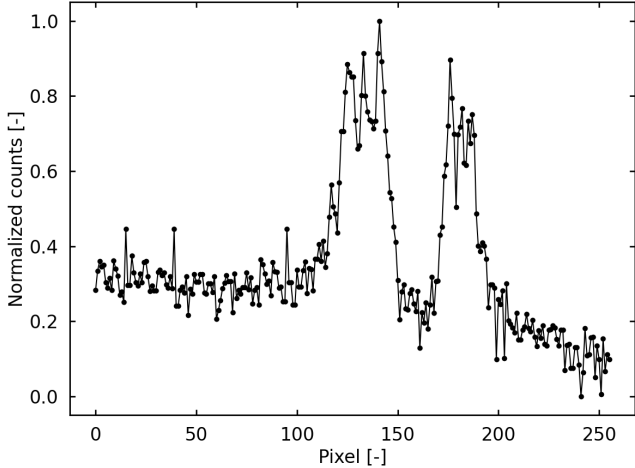


FIG. 5. Spectra of signal and idler photons from the SPDC source in the LinoSPAD2 sensor.

SPDC photons present a typical anti-correlation in wavelengths due to the energy conservation, i.e. $\hbar\omega_{\text{pump}} = \hbar\omega_{\text{signal}} + \hbar\omega_{\text{idler}}$. Fig. 6 shows the wavelengths

anti-correlation for the signal and idler photons for pairs within a 20 ns time window. The anti-correlation is clear and is a signature of the SPDC process, although more sophisticated SPDC sources may have engineered spectral properties [22].

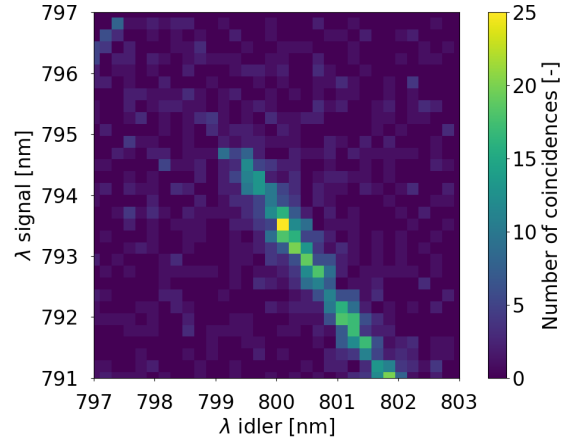


FIG. 6. Anti-correlation of wavelengths for signal and idler photons from the SPDC source.

D. Comparison to the Heisenberg Uncertainty Principle (HUP) limit

We compare the obtained resolution results to the limit determined by the Heisenberg Uncertainty Principle, which imposes resolution limits for joint measurement of two conjugate observables [25–28] and, therefore, is a useful benchmark to determine how close our spectrometer is to the ultimate quantum limit. The Heisenberg Uncertainty Principle does not limit the resolution for one of the observables alone but restricts the product of the uncertainty of two observables. For energy and time, it takes the form of:

$$\Delta E \Delta t \geq \frac{\hbar}{2}, \quad (1)$$

where \hbar is Planck's reduced constant, ΔE is the standard deviation for the measurement of energy, and Δt is the standard deviation for the measurement of time.

The uncertainty in energy can be estimated from the uncertainty in wavelength. Using $\Delta\lambda = 0.042$ nm for the 800.607 nm light and propagating the errors, we obtain $\Delta E = 8.1 \times 10^{-5}$ eV. The temporal uncertainty per photon is 40 ps, as estimated before. From the above, we estimate the product of the uncertainties in time and energy to be:

$$\Delta E \Delta t = 3.3 \times 10^{-15} \text{ eVs.} \quad (2)$$

Therefore, $(\Delta E \Delta t)/(\hbar/2) \approx 10$, which tells us that we are a factor of ten from the Heisenberg limit of $\hbar/2$.

We emphasize that this product of the resolutions is applicable to a single particle and that the spectrometer can simultaneously measure the energy and time for each photon detected in it, even if multiple photons are detected at the same time. Considering the simplicity and straightforwardness of our experimental setup, we believe that this represents a significant result.

An important clarification is that we directly measured the spectral resolution using the thermal light and we directly measured the temporal resolution using the SPDC light, and we assume that the same resolutions will be applicable to other photon generation mechanisms and different wavelengths in a reasonable range. Within these assumptions, we believe that we can use the Heisenberg Uncertainty Principle as a natural benchmark to evaluate the performance of this spectrometer, as the HUP imposes the ultimate quantum limit of resolution for a joint (simultaneous) measurement of energy and time for single particles.

II. DISCUSSION

We demonstrated a single photon detector and spectrometer with 0.04 nm spectral and 40 ps temporal resolution, based on the LinoSPAD2 sensor. The spectrometer resolution makes it a unique instrument capable of characterizing properties of single photons near the Heisenberg Uncertainty Principle limit, only ten times above it.

We note that the spectral resolution can be improved by employing the echelle gratings in which a standard first-order grating is used perpendicular to a second grating. High resolution is provided by the high-order diffraction, and the first-order grating vertically separates the overlapping modes. The output of an echelle spectrometer is a series of parallel stripes, so a two-dimensional array should be used to give high spectral resolution across a large range. The typical resolution for this type of spectrometer is around 0.01 nm, a possible improvement by a factor of 4 over our results.

The SPAD technology is also quickly progressing, improving the parameters relevant to the measurements described here: photon detection efficiency, timing resolution, and array size. In particular, a 7 ps timing resolution was demonstrated recently [29, 30], about a factor of 6 better than measured in this work. Two-dimensional 1 Mpixel SPAD arrays were produced and tested [2], though not with the data-driven readout as reported here. Fully reconfigurable two-dimensional SPAD-based cameras would ultimately be built using 3D-stacking technologies, whereby SPADs would be employed as photon-to-digital conversion elements, stacked onto CMOS-based reconfigurable circuitry in an FPGA-like bottom tier [17]. These future improvements will allow us to get even closer to the Heisenberg Uncertainty Principle limit.

Our work can help characterize single-photons

sources [22, 31], in particular their spectral properties and their implications for quantum interference [32–34]. Other areas that could also benefit are time-resolved spectroscopy [35], quantum metrology [36], time-domain quantum optical modes [37], and quantum spectroscopy [38]. The technology we demonstrated here has the potential to unlock many applications in both classical and quantum physics.

III. METHODS

In this section, we provide additional details about the setup and analysis.

A. Additional information on the spectrometer

The implemented spectrometer has a straightforward design employing a 1200 lines/mm diffraction grating and $f = 200$ mm lens. Before the grating, the incoming light is collimated with a lens producing a parallel beam of 2 mm diameter. The first-order reflections from the grating are focused on the sensor placed at the focal distance from the lens. The resulting conversion scale is 0.11 nm/pixel. Alignment of the spectrometer output with respect to the very thin linear LinoSPAD2 array, which needs to be done in three dimensions, was a difficult task. We are devising improved sensor architectures to alleviate this issue.

We employed a Newport 6030 Argon calibration lamp at 10 mA DC current as a source of thermal light. The lamp light was coupled into a single-mode fiber. We used a Thorlabs correlated photon-pair source based on spontaneous parametric down-conversion of 405 nm pump photons in a ppKTP crystal. The source provides fiber-coupled photon pairs with the pump photon power range from 0 to 150 mW.

B. Additional information on LinoSPAD2 sensor

The full LinoSPAD2 sensor consists of two halves, 256 pixels each, which have a separate readout with the Spartan-6 FPGA. The time stamping is performed by an array of 64 time-to-digital converters (TDC), implemented in the FPGA and shared between 256 channels. The TDCs consist of 35-element delay lines, where each element is made of a 4-bit carry chain block. The resulting 140-bit time code is sampled and encoded into an 8-bit number. The sampling frequency, derived from an external crystal oscillator, is 400 MHz at nominal conditions. A 20-bit counter operating at the same frequency expands the 8-bit code obtained from the TDC to a 28-bit timestamp with the least-significant bit (LSB) resolution of 17.875 ps. The longest possible acquisition cycle is 4 ms long, for which an internal trigger of 250 Hz is used. The pixel deadtime, i.e. the time after a detection for

which the pixel is insensitive to the another detection, is about 50 ns.

The FPGA internal block memory can store up to 512 timestamps per pixel per acquisition cycle. A USB 3.0 interface is used for communication and data exchange between the readout board and the acquisition computer. Given all the above parameters, the sensor and its acquisition system, as was used here, were able to time stamp a continuous stream of single photons and read them out to a computer with a maximum rate of 8M photons per second.

C. Data analysis and calibration

The data is analyzed by calculating the time difference between the timestamps of different SPAD pixels. Only timestamps from a single acquisition cycle are taken into account. Additionally, due to the TDC non-linearities and unequal time offsets for different pixels, the data must be adjusted using calibrations to account for these effects.

The TDC 140-bit output code, sampled at 400 MHz, covers a time window of 2.5 ns, with an average bin width of 17.857 ps. However, the actual width of each bin is different due to uneven propagation delays in the FPGA carry chain logic. In addition, due to the different trace lengths between each SPAD and the inputs of the TDCs, there is a static offset in timestamping that varies between different pixels. Two calibration procedures were therefore required. The first one was used to compensate for the non-linearity of each TDC, and the second one to compensate for the offset of each SPAD.

The non-linearity of each TDC has been calibrated using a code density test technique where the sensor is

homogeneously illuminated with a uniform light source. Ideally, this should result in all histogram bins being equally populated. In reality, the bins with larger propagation delays have higher occupancy, and bins with lower propagation delays have lower occupancy. The occupancy of individual bins directly gives the bin time width, assuming that the 140-bit code covers exactly 2.5 ns. Recalibrating the output data of each TDC compensates for the non-linearity and, thus, gives the real-time information of individual timestamps.

The offset of each SPAD was calibrated using a picosecond pulse laser flashing at the entire sensor. With the assumption that all SPADs should register photons at the same time, we compiled and solved a set of linear equations with corresponding time differences for all possible pixel pairs. This allowed us to determine the individual offset delays of each SPAD. The resulting calibration data, non-linearity, and time offsets were then used for the offline data analysis.

ACKNOWLEDGMENTS

This work was supported by the U.S. Department of Energy QuantISED award, the Brookhaven National Laboratory LDRD grant 22-22, the Ministry of Education, Youth and Sports of the Czech Republic Grant No. LM2023034, as well as from European Regional Development Fund-Project "Center of Advanced Applied Science" No. CZ.02.1.01/0.0/0.0/16-019/0000778. This work was also supported by the EPFL internal IMAGING project "High-speed multimodal super-resolution microscopy with SPAD arrays" and the DOE/LLNL project "The 3DQ Microscope". We are grateful to Duncan England, Yingwen Zhang and Dmitri Kharzeev for useful discussions.

[1] S. M. Sze, *Semiconductor devices: physics and technology* (John wiley & sons, 2008).

[2] K. Morimoto, A. Ardelean, M.-L. Wu, A. C. Ulku, I. M. Antolovic, C. Bruschini, and E. Charbon, *Optica* **7**, 346 (2020).

[3] S. Burri, Y. Maruyama, X. Michalet, F. Regazzoni, C. Bruschini, and E. Charbon, *Optics express* **22**, 17573 (2014).

[4] M. S. A. Shawkat, M. H. U. Habib, and N. McFarlane, *IEEE Transactions on Circuits and Systems I: Regular Papers* **65**, 3830 (2018).

[5] F. Marsili, V. B. Verma, J. A. Stern, S. Harrington, A. E. Lita, T. Gerrits, I. Vayshenker, B. Baek, M. D. Shaw, R. P. Mirin, *et al.*, *Nature Photonics* **7**, 210 (2013).

[6] R. Cheng, C.-L. Zou, X. Guo, S. Wang, X. Han, and H. X. Tang, *Nature communications* **10**, 4104 (2019).

[7] B. Korzh, Q.-Y. Zhao, J. P. Allmaras, S. Frasca, T. M. Autry, E. A. Bersin, A. D. Beyer, R. M. Briggs, B. Bumble, M. Colangelo, *et al.*, *Nature Photonics* **14**, 250 (2020).

[8] R. Cheng, Y. Zhou, S. Wang, M. Shen, T. Taher, and H. X. Tang, *Nature Photonics* **17** (2023).

[9] L. K. Shalm, E. Meyer-Scott, B. G. Christensen, P. Bierhorst, M. A. Wayne, M. J. Stevens, T. Gerrits, S. Glancy, D. R. Hamel, M. S. Allman, K. J. Coakley, S. D. Dyer, C. Hodge, A. E. Lita, V. B. Verma, C. Lambrocco, E. Tortorici, A. L. Migdall, Y. Zhang, D. R. Kumor, W. H. Farr, F. Marsili, M. D. Shaw, J. A. Stern, C. Abellán, W. Amaya, V. Pruneri, T. Jennewein, M. W. Mitchell, P. G. Kwiat, J. C. Bienfang, R. P. Mirin, E. Knill, and S. W. Nam, *Phys. Rev. Lett.* **115**, 250402 (2015).

[10] S. Slussarenko, M. M. Weston, H. M. Chrzanowski, L. K. Shalm, V. B. Verma, S. W. Nam, and G. J. Pryde, *Nature Photonics* **11**, 700 (2017).

[11] A. E. Lita, A. J. Miller, and S. W. Nam, *Opt. Express* **16**, 3032 (2008).

[12] L. A. Morais, T. Weinhold, M. P. de Almeida, J. Combes, A. Lita, T. Gerrits, S. W. Nam, A. G. White, and G. Gillett, "Precisely determining photon-number in real-time," (2020), arXiv:2012.10158.

[13] M. Eaton, A. Hossameldin, R. J. Birrittella, P. M. Alsing,

C. C. Gerry, H. Dong, C. Cuevas, and O. Pfister, *Nature Photonics* **17** (2023).

[14] L. Howard, G. Gillett, M. Pearce, R. Abrahao, T. Weinhold, P. Kok, and A. White, *Physical review letters* **123**, 143604 (2019).

[15] M. Giustina, M. A. M. Versteegh, S. Wengerowsky, J. Handsteiner, A. Hochrainer, K. Phelan, F. Steinlechner, J. Kofler, J.-A. Larsson, C. Abellán, W. Amaya, V. Pruneri, M. W. Mitchell, J. Beyer, T. Gerrits, A. E. Lita, L. K. Shalm, S. W. Nam, T. Scheidl, R. Ursin, B. Wittmann, and A. Zeilinger, *Phys. Rev. Lett.* **115**, 250401 (2015).

[16] S. Burri, H. Homulle, C. Bruschini, and E. Charbon, in *Optical Sensing and Detection IV*, Vol. 9899, edited by F. Berghmans and A. G. Mignani, International Society for Optics and Photonics (SPIE, 2016) p. 98990D.

[17] C. Bruschini, S. Burri, E. Bernasconi, T. Milanese, A. C. Ulku, H. Homulle, and E. Charbon, in *Quantum Sensing and Nano Electronics and Photonics XIX*, Vol. 12430 (SPIE, 2023) pp. 126–135.

[18] P. Stankus, A. Nomerotski, A. Slosar, and S. Vintskevich, *The Open Journal of Astrophysics* **5** (2022), 10.21105/astro.2010.09100.

[19] J. Crawford, D. Dolzhenko, M. Keach, A. Muenninghoff, R. A. Abrahao, J. Martinez-Rincon, P. Stankus, S. Vintskevich, and A. Nomerotski, “Towards quantum telescopes: Demonstration of a two-photon interferometer for quantum-assisted astronomy,” (2023), arXiv:2301.07042.

[20] A. Nomerotski, P. Stankus, A. Složar, S. Vintskevich, S. Andrewski, G. A. Carini, D. Dolzhenko, D. England, E. V. Figueroa, S. Gera, J. Haupt, S. Herrmann, D. Kastramatos, M. Keach, A. Parsells, O. Saira, J. Schiff, P. Svihra, T. Tsang, and Y. Zhang, in *Optical and Infrared Interferometry and Imaging VII*, Proc. SPIE, edited by A. Mérard, S. Sallum, and P. G. Tuthill (2020).

[21] A. Kramida, Yu. Ralchenko, J. Reader, and and NIST ASD Team, NIST Atomic Spectra Database (ver. 5.10), [Online]. Available: <https://physics.nist.gov/asd> [2023, March 6]. National Institute of Standards and Technology, Gaithersburg, MD. (2022).

[22] A. Christ, A. Fedrizzi, H. Hübel, T. Jennewein, and C. Silberhorn, in *Experimental Methods in the Physical Sciences*, Vol. 45 (Elsevier, 2013) pp. 351–410.

[23] B. Farella, G. Medwig, R. A. Abrahao, and A. Nomerotski, “(private communication) *In preparation*,”.

[24] A. Nomerotski, M. Chekhlov, D. Dolzhenko, R. Glazeborg, B. Farella, M. Keach, R. Mahon, D. Orlov, and P. Svihra, *Journal of Instrumentation* **18**, C01023 (2023).

[25] W. Heisenberg, *The physical principles of the quantum theory* (Courier Corporation, 1949).

[26] J. Sakurai and J. Napolitano, Person New International edition , 35 (2014).

[27] B. C. Hall, *Quantum theory for mathematicians* (Springer, 2013).

[28] H. P. Robertson, *Phys. Rev.* **34**, 163 (1929).

[29] F. Gramuglia, M.-L. Wu, C. Bruschini, M.-J. Lee, and E. Charbon, *IEEE Journal of Selected Topics in Quantum Electronics* **28**, 1 (2022).

[30] F. Gramuglia, E. Ripicci, C. A. Fenoglio, M.-L. Wu, L. Paolozzi, C. Bruschini, and E. Charbon, *Frontiers in Physics* **10** (2022), 10.3389/fphy.2022.849237.

[31] P. Senellart, G. Solomon, and A. White, *Nature nanotechnology* **12**, 1026 (2017).

[32] C. K. Hong, Z. Y. Ou, and L. Mandel, *Phys. Rev. Lett.* **59**, 2044 (1987).

[33] T. Kobayashi, R. Ikuta, S. Yasui, S. Miki, T. Yamashita, H. Terai, T. Yamamoto, M. Koashi, and N. Imoto, *Nature photonics* **10**, 441 (2016).

[34] K. M. Jordan, R. A. Abrahao, and J. S. Lundeen, *Phys. Rev. A* **106**, 063715 (2022).

[35] G. Lubin, R. Tenne, A. C. Ulku, I. M. Antolovic, S. Burri, S. Karg, V. J. Yallapragada, C. Bruschini, E. Charbon, and D. Oron, *Nano Letters* **21**, 6756 (2021), pMID: 34398604.

[36] V. Giovannetti, S. Lloyd, and L. Maccone, *Nature photonics* **5**, 222 (2011).

[37] M. G. Raymer and I. A. Walmsley, *Physica Scripta* **95**, 064002 (2020).

[38] S. Mukamel, M. Freyberger, W. Schleich, M. Bellini, A. Zavatta, G. Leuchs, C. Silberhorn, R. W. Boyd, L. L. Sánchez-Soto, A. Stefanov, *et al.*, *Journal of physics B: Atomic, molecular and optical physics* **53**, 072002 (2020).